Fluorescence resonance energy transfer links membrane ferroportin, hephaestin but not ferroportin, amyloid precursor protein complex with iron efflux

Received for publication, July 31, 2018, and in revised form, January 8, 2019 Published, Papers in Press, January 15, 2019, DOI 10.1074/jbc.RA118.005142

Adrienne C. Dlouhy, Danielle K. Bailey, Brittany L. Steimle, Haley V. Parker, and Daniel J. Kosman[1]

From the Department of Biochemistry, Jacobs School of Medicine and Biomedical Sciences, University at Buffalo, Buffalo, New York 14203

Edited by Ruma Banerjee

Iron efflux from mammalian cells is supported by the synergistic actions of the ferrous iron efflux transporter, ferroportin (Fpn) and a multicopper ferroxidase, that is, hephaestin (Heph), ceruloplasmin (Cp) or both. The two proteins stabilize Fpn in the plasma membrane and catalyze extracellular Fe^{3+} release. The membrane stabilization of Fpn is also stimulated by its interaction with a 22-amino acid synthetic peptide based on a short sequence in the extracellular E2 domain of the amyloid precursor protein (APP). However, whether APP family members interact with Fpn *in vivo* is unclear. Here, using cyan fluorescent protein (CFP)-tagged Fpn in conjunction with yellow fluorescent protein (YFP) fusions of Heph and APP family members APP, APLP1, and APLP2 in HEK293T cells we used fluorescence and surface biotinylation to quantify Fpn membrane occupancy and also measured ^{59}Fe efflux. We demonstrate that Fpn and Heph co-localize, and FRET analysis indicated that the two proteins form an iron-efflux complex. In contrast, none of the full-length, cellular APP proteins exhibited Fpn co-localization or FRET. Moreover, iron supplementation increased surface expression of the iron-efflux complex, and copper depletion knocked down Heph activity and decreased Fpn membrane localization. Whereas cellular APP species had no effects on Fpn and Heph localization, addition of soluble E2 elements derived from APP and APLP2, but not APLP1, increased Fpn membrane occupancy. We conclude that a ferroportin-targeting sequence, (K/R)EWEE, present in APP and APLP2, but not APLP1, helps modulate Fpn-dependent iron efflux in the presence of an active multicopper ferroxidase.

Systemic mammalian iron balance is maintained primarily at the point of iron release into the portal vein at the basolateral membrane of the intestinal epithelium (1–3). Modulation of this epithelial iron release is achieved by regulation of the residence of the sole iron efflux transporter, ferroportin (Fpn),[2] in this membrane. Two proteins are broadly recognized to contribute to the membrane occupancy of Fpn: 1) the multicopper ferroxidase, hephaestin (Heph), a type Ia membrane protein expressed by enterocytes (among other tissues) that appears to interact with Fpn and likely retards Fpn's normal retrograde internalization (4–7); and 2) hepcidin, a peptide hormone secreted primarily by the liver, that binds to Fpn, triggering Fpn's ubiquitination and degradation (8–13). This dual regulatory pattern appears to obtain irrespective of the cell type involved, *e.g.* intestinal enterocytes or the macrophages that recycle red cell iron where circulating ceruloplasmin (sCp) complements the activity of hephaestin (1, 2, 14, 15). This latter pattern is found also in the abluminal space in the brain where sCp and its GPI-linked, plasma membrane tethered form function together with Heph in managing iron trafficking in the neurovascular unit (6, 16–18).

Fpn membrane occupancy has been linked to the iron and copper status of the cell as well. Thus, in cells made copper-limited by treatment with Cu(I) chelating agents like bathocuproine disulfonate (BCS) or tetrathiomolybdate membrane Fpn declines as does iron efflux as a result of the decrease in copper-replete, active Heph (6, 19, 20). A similar Fpn down-regulation has been reported in cells from Cp knockout mice (21). The effect of iron is less clear with reports of an increase (22, 23) or a decrease (5) in Fpn surface expression in response to iron supplementation. Certainly, the former response would be expected given the role Fpn has in iron efflux; in any case the mechanism of the response remains unclear.

Recently, a third Fpn–protein interaction that modulates Fpn membrane occupancy has been identified, one likely critical to brain iron homeostasis. Bush and co-workers (24) demonstrated that hippocampal neuron Fpn was pulled-down by soluble amyloid precursor protein (sAPP) and presented data that indicated the presence of APP correlated with an increase in cell iron efflux. The mechanism underlying this correlation subsequently was demonstrated to be the result of a sAPP–Fpn

This work was supported by National Institutes of Health NINDS Grants RO3NS095063 and RO1NS102337, from the Department of Health and Human Services USA (to D. J. K.). The authors declare that they have no conflicts of interest with the contents of this article. The content of this article is solely the responsibility of the authors and does not necessarily represent the official views of the National Institutes of Health.

[1] To whom correspondence should be addressed: Suite 4102, 955 Main St., Buffalo NY 14203. Tel.: 716-829-2317; Fax: 716-829-2726; E-mail: camkos@buffalo.edu.

[2] The abbreviations used are: Fpn, ferroportin; Heph, hephaestin; (s)Cp, (soluble) ceruloplasmin; APP, amyloid precursor protein; APLP, amyloid precursor-like protein; FTP, ferroportin-targeting peptide; BCS, bathocuproine disulfonate; FRET, fluorescence resonance energy transfer; FAS, ferrous ammonium sulfate; FZ, ferrozine; ROI, regions of interest; PEI, polyethylenimine; GPI, glycosylphosphatidylinositol; CFP, cyan fluorescent protein; YFP, yellow fluorescent protein: GFP, green fluorescent protein.

interaction that increased Fpn membrane occupancy in brain microvascular endothelial cells and in the presence of a multicopper ferroxidase, a quantifiable increase in the rate of iron efflux (6, 25). Thus, in the abluminal space in the brain, sAPP appeared to suppress the negative regulation of Fpn function due to the hepcidin released from adjacent glial cells (16, 25). Previous studies had established the fact that the APP transcript includes a 5′ iron response element to which the iron response protein 1 bound when iron depleted inhibiting APP synthesis (26, 27). These findings suggested a role for APP in iron metabolism in the brain, a *physiologic* function for this protein most commonly considered in terms of its part in the *pathology* of neurodegenerative disease (28). Indeed, "Not just amyloid," the title of a recent review (29), reflects on the neurotrophic functions of the amyloid protein family.

Compelling evidence for a physiologic function(s) for APP is the fact that the APP, APLP2 and APLP1, APLP2 double knockout mouse strains die perinatally; APLP1 and APLP2 are the two APP paralogues. Significantly, *only* these double KO mouse lines had such a significant phenotype; all other single and double deletions involving these three genes gave rise to limited or only moderate physiologic deficiencies, *e.g.* the APP^{null}/$APLP1^{null}$ strain (29–33). These differences indicate that APP and APLP2, and APLP1 and APLP2 are redundant with respect to one or more essential processes. In the case of APP and APLP2 this includes a role in dendritic architecture, hippocampal long-term potentiation, and thus overall synaptic plasticity. Importantly, these functions appear to be due to the action of sAPPα and not the endogenous, full-length protein (34).

With respect to brain iron metabolism (24, 25, 28, 35), among the sequence motifs expressed in APP and APLP2 and *not* in APLP1 is the one associated with sAPP binding to Fpn (24, 25), a sequence referred to as the "ferroportin targeting peptide" (FTP) (25). This motif is found in the E2 domains of APP and APLP2 (Fig. 1*A*); the sequences shown in Fig. 1*C* illustrate the sequence homology between APP and APLP2 and the differences in the APLP1 protein, whereas Fig. 1*B* illustrates the FTP motif in the proteins' E2 domain αBαC helical motifs. The 22-amino acid FTP in the β-amyloid A4 protein (APP) and its isoforms is 100% conserved in all archived mammalian genomes.

In this report, using HEK293 cells as host, we probed the co-localization of and potential FRET between fluorescently-tagged fusions of Fpn, Heph, and the three APP family members. Co-localization and FRET analyses demonstrate that Fpn and Heph traffic together to the plasma membrane, whereas Fpn and APP do not. We demonstrate that iron treatment stimulates increased FRET between Fpn-CFP and Heph-YFP and an increase in surface-exposed Fpn. In contrast, depletion of Heph function by copper chelation results in a decrease in both Fpn cell-surface occupancy and iron efflux. Although cell-associated, unprocessed APP family members do not influence plasma membrane localization of Fpn-CFP, the αBαC helical motifs from APP and APLP2 stimulate the membrane presentation of Fpn and iron efflux, whereas this protein domain from APLP1 does not. These data suggest that in the brain interstitium APP and APLP2 in their soluble forms, along with sCp (6, 16), play a specific *agonist* role in ferroportin function in contrast to the *antagonist* role played by hepcidin.

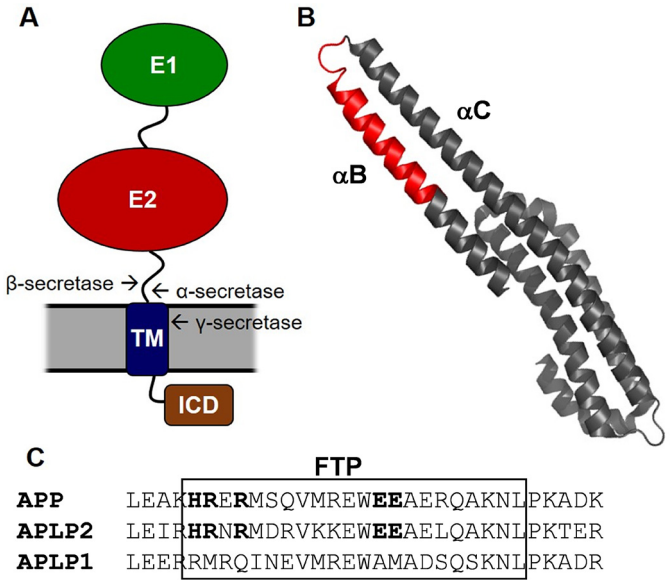

Figure 1. The APP–Fpn interaction structural motifs. *A*, schematic of domain organization of APP and its orthologues with APP secretase-processing sites indicated. The E1 and E2 elements comprise the APP ectodomain. *B*, the E2 domain and its five helical motifs. The FTP binding sequence (shown in *C*) is highlighted in *red* and is found at the C-terminal end of the αB helix. The αBαC domains were the recombinant proteins used in this report; in APP this domain consists of residues 318–408. The structure shown is from Protein Data Bank 3UMH. *C*, the FTP sequence in APP and APLP2 and the corresponding residues in APLP1. The FTP sequence is *boxed* with the residues targeted as FTP-specific in *bold*.

Results

FRET analysis of ferroportin, hephaestin, and APP family member interaction

HEK293T cells were used as host for the expression of a C-terminal CFP fusion of Fpn, and C-terminal YFP fusions of Heph, APP, APLP1, and APLP2; the C termini of all these proteins have a cytoplasmic orientation (36–38). HEK293 cell lines have been used extensively for examination of the trafficking of Fpn and Heph (37, 39–43) and GFP fusions Fpn and Heph have been used effectively in examining the trafficking of these proteins individually in HEK293, HeLa, and Caco-2 cells (23, 44, 45). In addition, iron efflux due to episomally-encoded Fpn has been demonstrated in HEK293 cells (37, 46). Examination by epifluorescence of transfected cells expressing Fpn-CFP along with one of the four YFP fusions indicated co-localization of Fpn only with Heph (Fig. 2). A major fraction of the Fpn-CFP was observed in the plasma membrane along with Heph-YFP.

We appreciate that cyan and yellow fluorescent markers make poor reagents for co-localization analyses. Our use of these fluors were dictated by our principal objective of obtaining evidence for energy transfer between them to provide higher resolution of protein–protein interaction than that afforded by the merging of two fluorescent images. Thus, using confocal microscopy, the potential association of Fpn-CFP with one or more of the four YFP protein fusions was probed by FRET analysis. In this experiment, FRET efficiency was quantified by the increase in donor fluorescence following photobleaching of the acceptor fluor. A sample of the images obtained in such an experiment with the Heph-YFP fusion is shown in Fig. 3; for FRET quantification, membrane-associated

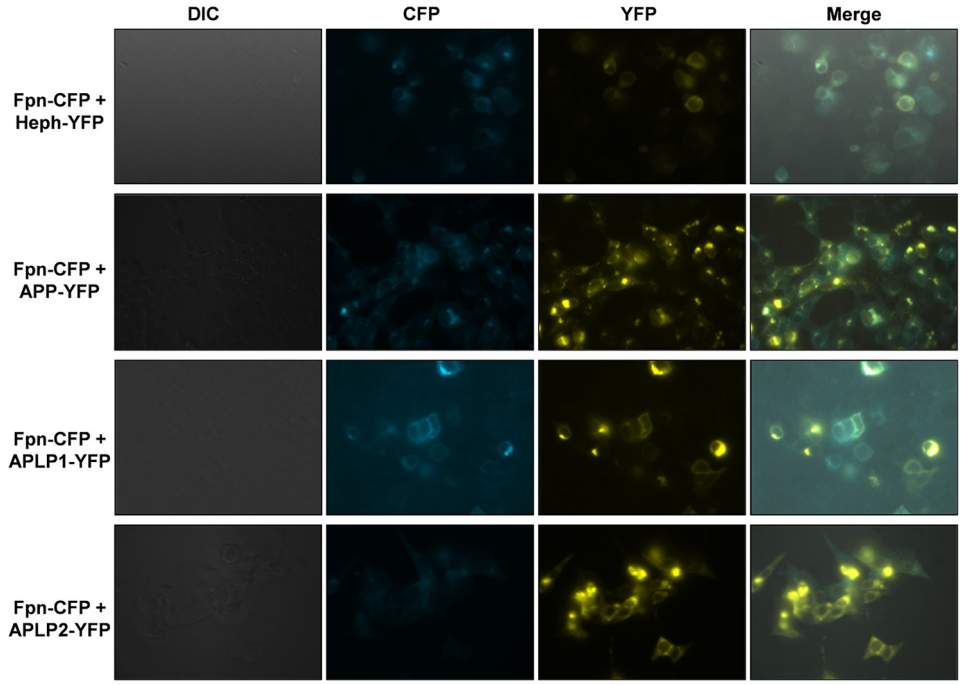

Figure 2. Localization of fluorescent fusions of Fpn, Heph, APP, APLP1, and APLP2. Epifluorescence images of HEK293T cells co-transfected with plasmids expressing Fpn-CFP and -YFP fusions of potential partner proteins. Fpn and Heph fusions localize to the plasma membrane, whereas the fusions of APP and its paralogues are predominantly found in intracellular compartments. Cells were fixed with 4% paraformaldehyde, 4% sucrose in PBS 48 h after transfection. Images were obtained on a Zeiss AxioImager fluorescence microscope using a ×10 objective.

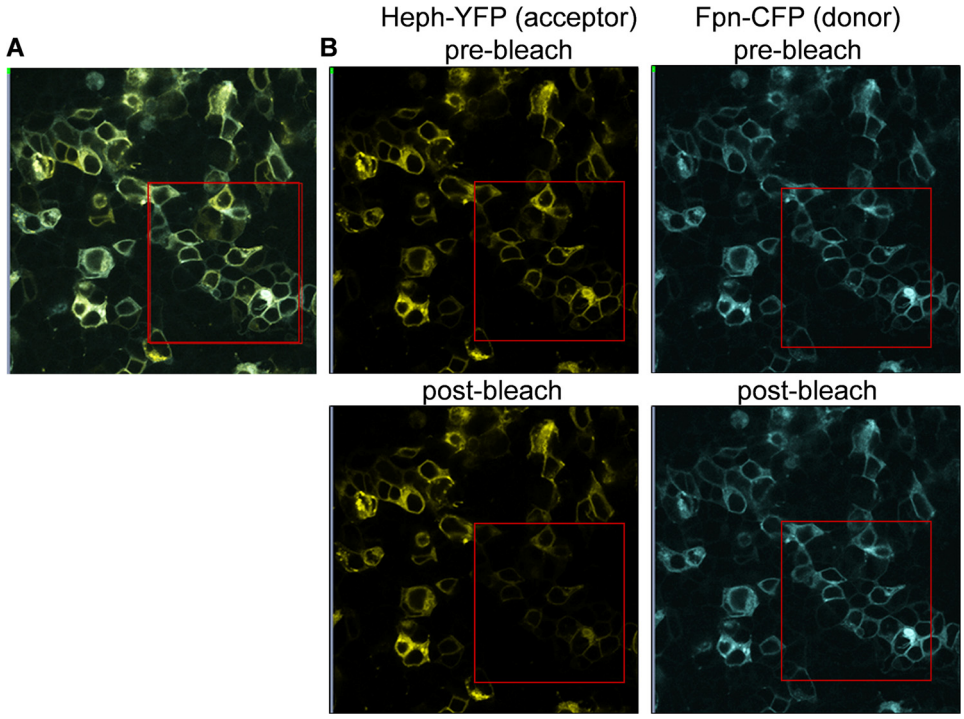

Figure 3. Acceptor photobleaching to assess Fpn-CFP, Heph-YFP FRET. *A*, merged image shows both YFP and CFP fluorescence after photobleaching the acceptor. *B*, YFP channel showing fluorescence from Heph-YFP fusion before and after photobleaching the acceptor (*left panels*). CFP channel showing fluorescence from Fpn-CFP fusion before and after photobleaching the acceptor (*right panels*). The bleached field is indicated by the *red box*; FRET intensities were quantified in the ROI confined to membrane contiguous spaces within these bleached areas. The data were obtained on a Zeiss LSM 510 Meta confocal microscope using the FRET+ macro.

regions of interest (ROI) were isolated from such fields. Table 1 provides the estimates of the Fpn-Heph proximity based on the standard R_0 value for the CFP-YFP pair (47). As discussed later, this distance value is likely an overestimate because it is based on a FRET efficiency that has not been corrected for the fraction of Fpn-CFP in an ROI that is *not* in association with Heph-YFP (48).

In contrast to the apparent co-localization of and the FRET quantified between Fpn-CFP and Heph-YFP, there was little or

Table 1
Calculated FRET efficiency for the Fpn-CFP + Heph-YFP interaction

FRET efficiency is measured as the percent increase in donor fluorescence intensity (CFP) upon photo-bleaching of the acceptor (YFP). FRET efficiency in cells in which the acceptor was not photobleached (unbleached, cells outside of the boxed areas), and in photobleached cells expressing only Fpn-CFP are reported as negative controls. The negative results obtained with YFP-derivatives of APP family members are noted. Mean ± S.D. are based on at least three independent cell measurements from each of three or more different images. *R* (Å) is the distance between donor and acceptor fluors, based on an R_0 of 50 Å for the CFP-YFP pair.

Interrogated protein(s)	FRET efficiency	*R*
	%	Å
Fpn-CFP + Heph-YFP	8.16 ± 2.97	74.5
Fpn-CFP + Heph-YFP (unbleached field)	3.29 ± 2.76	NS[a]
Fpn-CFP alone	1.90 ± 1.04	NS
Fpn-CFP + APP-YFP (also, APLP1, APLP2)	Variable, −1 to +1	

[a] NS, not significant, estimated values greater than 120 Å.

no co-localization apparent between Fpn-CFP and any of the YFP fusions of APP and its orthologues (Fig. 2). Although these images were not subject to fluorescence quantification, there was somewhat more APLP1-YFP than YFP-tagged APP and APLP2 visualized at the cell surface. These results on this differing locale of fluorescently-tagged APP and its orthologues expressed in HEK293 cells were in agreement with those reported by the Multhaup group (49).

More significantly, there was no FRET quantifiable between Fpn-CFP and any of the APP family member YFP fusions (Table 1). This result suggests that *cellular*, full-length APP likely plays a minor if any role in the localization or activity of Fpn in iron efflux at the plasma membrane. A similar finding was described in primary hippocampal neurons in which APP was knocked-down by an iRNA approach (19). Note that the C-terminal, cytoplasmic domains to which the fluors were appended in Fpn, Heph, and the APP proteins were of comparable length (35–45 residues); thus, the lack of FRET between the latter species and Fpn-CFP cannot readily be ascribed to a difference in linker-length between Heph and the APP proteins.

Cell iron status: effect on Fpn, Heph localization

There are conflicting reports about the localization of Fpn as a function of cell iron status; iron repletion has been correlated with both an increase (23, 50) and decrease (5, 51) in plasma membrane localization of this iron efflux protein. We used our fluorescent fusion proteins to quantify the effect of iron treatment both in regards to Fpn localization and Fpn-CFP, Heph-YFP association. In these experiments, to complement fluorescence imaging, Fpn plasma membrane surface occupancy was quantified by biotinylation and subsequent pulldown of the biotinylated surface proteins.

The data in Fig. 4 illustrate the effect on Fpn-CFP and Heph-YFP localization as a result of treatment with 10 μM ferrous ammonium sulfate (FAS). In Fig. 4*A*, the trafficking of the two proteins is visualized qualitatively and indicates an increase in plasma membrane occupancy of both proteins at 2 h post-iron treatment. Corresponding to the qualitative increase in CFP and YFP membrane fluorescence was a quantifiable 30% increase in FRET efficiency 2 h post-treatment (Fig. 4, *B* and *C*) (Table 2). This difference was attenuated at 4 h post-iron treatment and was clearly lost at 8 h. Reasonably, the increase in FRET efficiency is likely due to an increase in the fraction of the Fpn-CFP in association with the partner fluor, but does not explicitly report on the fraction in the plasma membrane.

In contrast, the biotinylation data provide a quantifiable pattern of change in surface Fpn following iron treatment. In cells expressing both proteins, a 3-fold increase in surface Fpn-CFP was quantified 4 h post-iron addition (Fig. 5*A*). In contrast, when Fpn-CFP was expressed alone, iron treatment stimulated a ~3-fold increase in plasma membrane localization at 2 h post-treatment (Fig. 5*B*). Note that the abundance of both total and surface-localized Fpn-CFP in these experiments was *independent* of the co-expression of Heph-YFP ($t = 0$ values in Fig. 5, *A* and *B*).

Overall, these data are consistent with previous reports indicating an increase in Fpn membrane occupancy in iron-replete cells (23, 50). In this regard, the effect of iron is the inverse of the down-regulation of this membrane localization caused by hepcidin (9, 52, 53). A caveat in comparing results like these is that the effect of any endocrine modulation of Fpn localization could be cell-type specific. For example, this programming might be different in a polarized barrier cell compared with the HEK293 cells used here.

We note the temporal difference in Fpn surface localization as quantified by biotinylation (Fig. 5*A*), which peaks at 4 h post-treatment, *versus* the increase in Fpn-CFP, Heph-YFP FRET at 2 h (Fig. 4). One possible explanation is that the latter increase is due partially to cytoplasmic and not a plasma membrane-localized complex. Another contributor to this difference is simply the temporal differences in the application of the two techniques. For the image analysis, cells are fixed at the times indicated, whereas in surface biotinylation, the time noted indicates reagent addition with a following incubation period only after which the cells are lysed. None the less, the FRET and surface biotinylation data support the premise that the initial effect of iron treatment is to stimulate an increase in the abundance of an Fpn-CFP, Heph-YFP complex.

Cell copper status: effect on Fpn, Heph localization, ferroxidase activity, and ^{59}Fe efflux

Several studies have demonstrated that Fpn plasma membrane presentation correlates with the level of endogenous Heph or GPI-linked Cp, or exogenous sCp (6, 16, 25). The level of Heph is depressed in cells made copper-limited by treatment with one or more copper chelators, *e.g.* BCS (membrane impermeant) and tetrathiomolybdate (membrane permeant) (6, 54–56). We examined the cell locale of Fpn-CFP and Heph-YFP in cells treated with BCS, and quantified the effect of copper depletion on the fractional loss of ^{59}Fe over a 24-h period. The epifluorescence images shown in Fig. 6 demonstrate the expected effect of Cu(I) chelation, namely a relative decrease in plasma membrane-localized Heph and Fpn. The effect of the BCS treatment on efflux of cell iron is quantified by the data shown in Fig. 7*A*. First, note HEK cells episomally expressing Fpn-CFP only (no co-expression of Heph-YFP) exhibit a 3-fold greater ^{59}Fe-efflux capacity than untransfected, control cells. Significantly (albeit unexpectedly), co-expressing Heph-YFP did not support an increase in loss of ^{59}Fe in 24 h. Nonetheless, the effect of Cu(I) chelation did correlate with the level of *total* cell Heph wherein BCS knocks down iron efflux more effec-

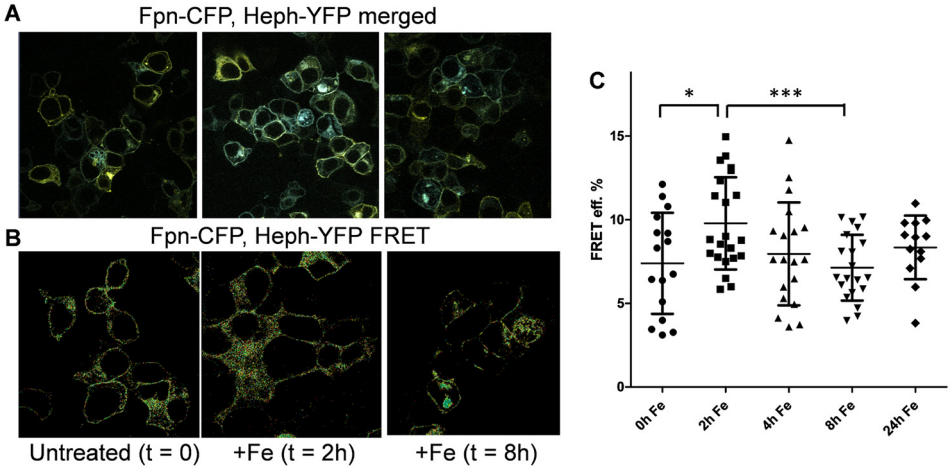

Figure 4. FRET efficiency in HEK cells expressing Fpn-CFP, Heph-YFP following iron treatment. HEK293T cells were transfected with both Fpn-CFP and Heph-YFP plasmids. Forty-eight hours post-transfection, cells were treated with 10 μM FAS for 0, 2, 4, 8, or 24 h before being fixed with 4% paraformaldehyde, 4% sucrose in PBS. *A*, Fpn-CFP, Heph-YFP merged images after iron treatment for the time periods as indicated. *B*, heat maps of FRET between Fpn-CFP, Heph-YFP; *C*, FRET values were quantified as described in Fig. 3 at each time point. In the scatter plot, *, $p < 0.05$; ***, $p < 0.005$. The values for FRET efficiencies and corresponding *R* values are given in Table 2. As in Fig. 3, these images were acquired on a Zeiss LSM 510 Meta confocal microscope.

Table 2
Fpn-CFP, Heph-YFP FRET efficiencies following iron treatment
Data analysis as described in Table I.

Time (h)	FRET efficiency	*R*
	%	Å
0	7.39 ± 3.02	76.2
2	9.38 ± 3.30	73.0
4	7.42 ± 3.37	76.1
8	6.90 ± 2.19	77.1
24	7.07 ± 3.24	76.8

tively in cells expressing *only* endogenous (less) Heph than in cells overexpressing this plasmid-encoded multicopper ferroxidase along with Fpn-CFP.

We were cognizant of the fact that our "efflux" protocol did not specifically interrogate the *velocity* of cell iron loss in that we quantified the fraction of iron lost at a single 24-h time point. Thus, our analysis may have reported only on a fixed, maximal loss of ^{59}Fe; the fact that co-expression of Heph-YFP did not support an increase in efflux would be consistent with this view. An inherent limitation in our protocol is that efflux experiments are conducted in cells that differ in total accumulated ^{59}Fe, differences that would mask the inherent activity of the efflux complex. However, any change in this *specific* efflux activity reasonably would be reflected in a difference in ^{59}Fe accumulation over the 24-h loading period. The data in Fig. 7*B* are consistent with the inference that, for example, co-expression of Heph-YFP did, in fact, result in an apparent increase in efflux in as much as cells expressing both Fpn-CFP and Heph-YFP *retained* 30% less ^{59}Fe after 24 h compared with cells expressing Fpn-CFP alone.

To support the inference above concerning the relative abundance of Heph *activity* in control *versus* cells transfected with Heph-CFP, we quantified the total ferroxidase activity in both mock-transfected cells and those expressing Heph-YFP as well as the effect of BCS treatment. In the ferroxidase quantification of a cell extract, we compared the loss (oxidation) of ferrous iron as probed using the Fe(II)-specific chelator, ferrozine (FZ) with a standard curve based on hCp as a control ferroxidase. These data are provided in the inset in Fig. 7*A* and are

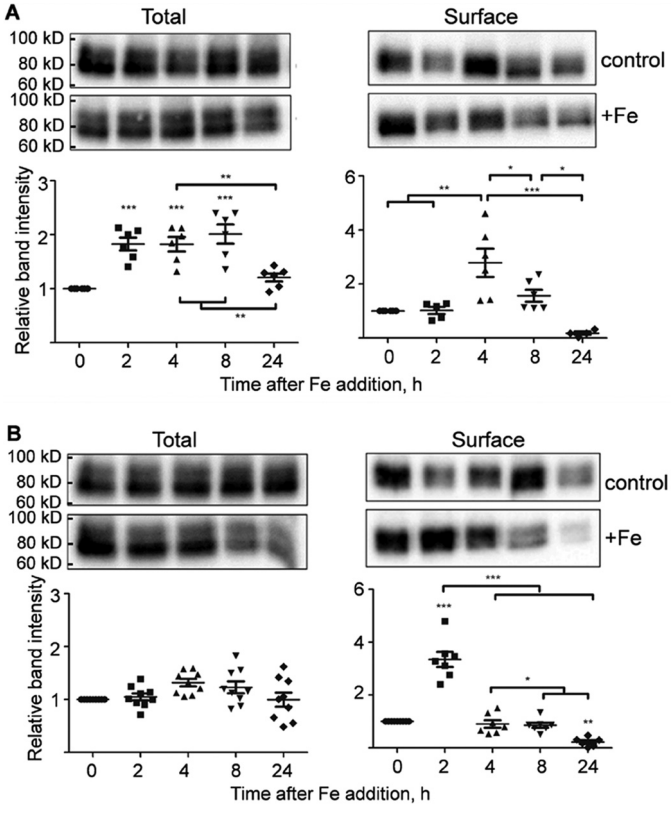

Figure 5. Effect of iron on surface expression of Fpn-CFP as determined by biotinylation. HEK293T cells were transfected with plasmids encoding Fpn-CFP and Heph-YFP (*panel A*) or Fpn-CFP alone (*panel B*). Forty-eight hours post-transfection, cells were treated with 10 μM FAS for 0, 2, 4, 8, or 24 h before being treated with EZ-Link Sulfo-NHS-SS-Biotin to biotinylate proteins at the cell surface. Control cells were untreated with FAS. Biotinylated proteins were pulled down with a Neutravidin column. Samples were probed for surface Fpn-CFP expression and compared with Fpn-CFP in total cell extracts; a rabbit anti-GFP antibody was used as probe in these blots. Duplicate blots were probed with anti-Fpn as an Fpn-specific control ("Experimental procedures"). For the "total" samples, 10 μg of protein were loaded in each lane; for "surface" the load represented a constant fraction of "input" to the Neutravidin column. The Western blotting data were quantified using Image Lab (Bio-Rad), and the intensities of the Fpn-CFP bands are reported relative to $t = 0$ h. The statistical analyses are of data derived from at least three experimental replicates. The blots shown are representative of the quality of the results.

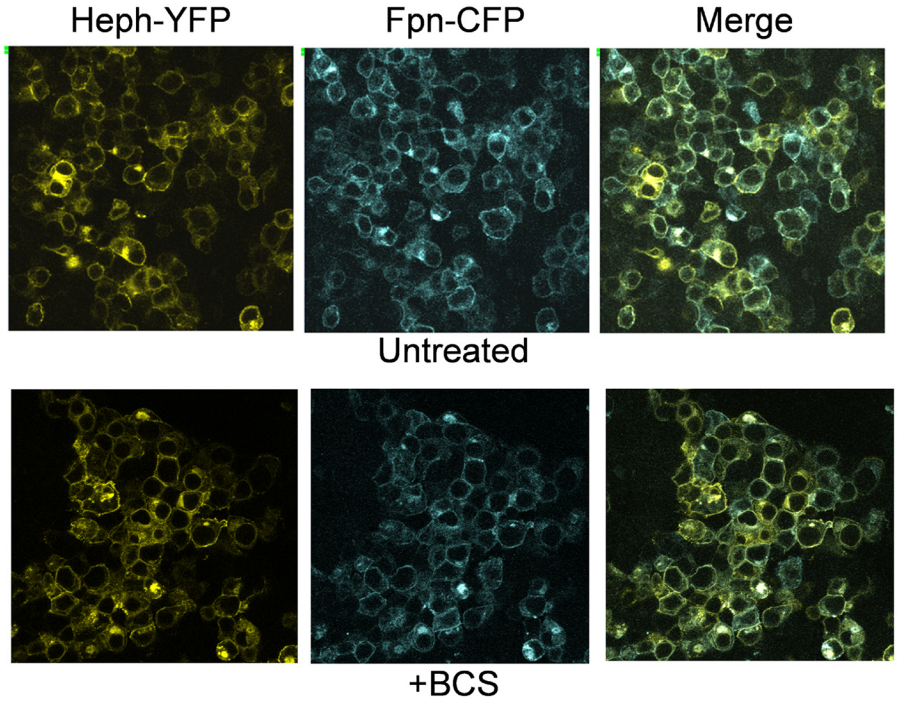

Figure 6. Localization of Fpn-CFP, Heph-YFP as a function of cell copper status. HEK293T cells co-transfected with plasmids expressing Fpn-CFP and Heph-YFP were treated with 500 μM BCS for 48 h before being fixed with 4% paraformaldehyde, 4% sucrose in PBS. Images were obtained on a Zeiss LSM 510 Meta confocal microscope using a ×40 objective.

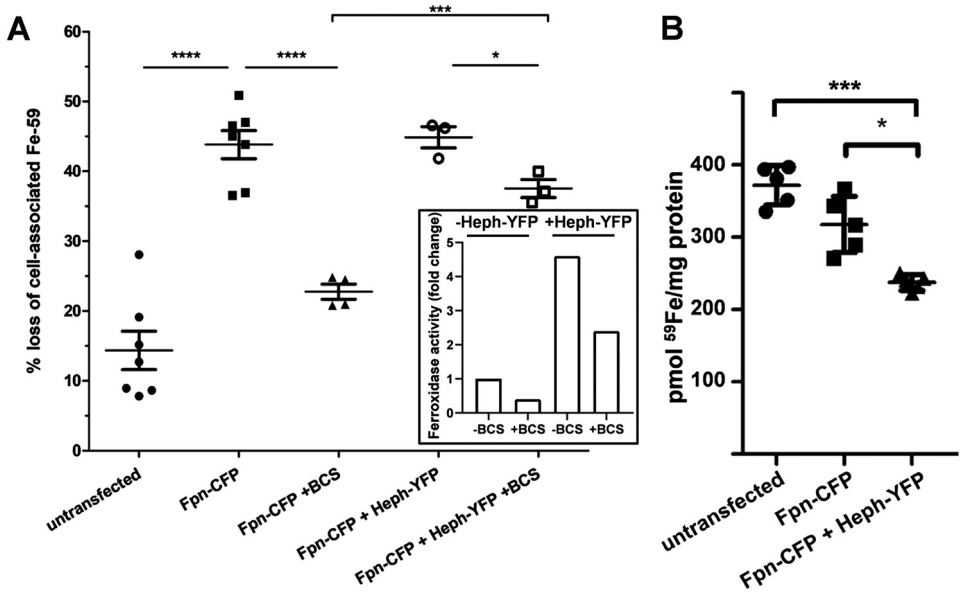

Figure 7. ^{59}Fe efflux as a function of hephaestin ferroxidase activity. HEK293T cells were transfected with the Fpn-CFP plasmid alone or with both Fpn-CFP and Heph-YFP plasmids. Forty-eight hours post-transfection, treated samples were incubated with 500 μM BCS for 24 h at which point all cells were treated with 1 μM $^{59}FeCl_3$ (plus citrate and ascorbate) for 24 h, then washed three times with the citrate uptake buffer. Lysates were prepared from a set of these $t = 0$ samples (representative data presented in *B*) and then from cells following a 24-h efflux period (data presented in *A*). The ^{59}Fe in all lysates was quantified by γ counting. Percent loss of cell-associated ^{59}Fe following the 24-h efflux period is reported relative to the initial accumulated metal ($t = 0$ h samples). The *inset* quantifies the relative ferroxidase activity in the Fpn-CFP transfectants, either control cells or those co-expressing Heph-YFP. The values are reported as fold-difference compared with the −BCS, Fpn-CFP sample (see "Experimental procedures"). Mean ± S.D. are based on three independent experiments. *, $p < 0.05$; ***, $p < 0.005$; ****, $p < 0.001$.

reported as the fold-difference compared with the minus BCS, Fpn-CFP expressing cells. These measured activities are consonant with the conclusions above but do not precisely delineate the correlation between this activity and Fpn iron-efflux efficiency. One caveat to our use of these episomally-encoded fusions is that, for example, expressed Heph-YFP may traffic to the plasma membrane inefficiently and thus express ferroxidase activity that does not contribute to Fpn function.

sAPP and its paralogues: effect on Fpn and Heph localization

A primary objective of this research was to examine the effect of sAPP and its proposed FTP-containing E2 domain on the

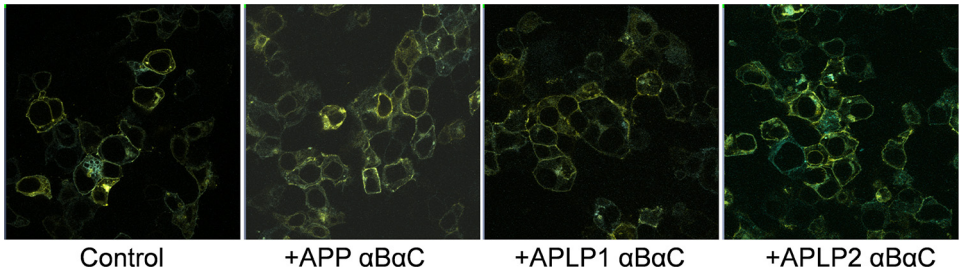

Figure 8. Localization of Fpn-CFP, Heph-YFP in response to addition of FTP and APP orthologues. HEK293T cells co-transfected with plasmids expressing Fpn-CFP and Heph-YFP were treated with 10 nM APPαBαC, APLP1αBαC, or APLP2αBαC for 48 h before being fixed with 4% paraformaldehyde, 4% sucrose in PBS. The merged images were obtained on a Zeiss LSM 510 Meta confocal microscope using a ×63 objective. Note that the control illustrated is the same control provided in Fig. 4*A*; the data for the FRET analyses shown in Fig. 4 and imaging of the samples shown here were collected during the same confocal session.

surface localization of the Fpn, Heph iron-efflux complex. We sought to answer two questions. First, did the unprocessed, intracellular forms of any of the APP family members modulate this surface localization and/or interact with it. The results presented above indicate that none of these APP proteins do. Second, we wished to test the prediction that among the soluble forms of these APP proteins, sAPLP2 and not sAPLP1 was physiologically redundant with sAPP in stimulating Fpn, Heph cell-surface presentation. To answer the latter question, we expressed and purified the αBαC helical domains of the three APP orthologues (see "Experimental procedures") and evaluated their activity in stabilizing the Fpn-CFP, Heph-YFP complex in the plasma membrane and in stimulation of ^{59}Fe efflux. We compared these effects to those obtained using the 22-residue FTP previously demonstrated to promote iron efflux in brain microvascular endothelial cells (25). The effect of these three recombinant helical domains on Fpn-CFP, Heph-YFP localization is shown in Fig. 8; the images are consistent with the premise that FTP elements in the αBαC motifs from APP and APLP2 increase plasma membrane localization of both proteins, an effect not shared by the APLP1-derived species that lacks this peptide sequence.

This premise was supported by quantification of Fpn-CFP surface biotinylation as shown in Fig. 9. Indeed, all three species containing the proposed FTP-specific sequence, REWEE, increased Fpn surface expression 2–3–fold. These results are in contrast to those involving the heterologous co-expression of APP-YFP and Heph-YFP; that is, as noted above, we found no evidence for co-localization of or FRET between the APP and Fpn fusions.

sCp and APPαBαC: effect on iron efflux

The ^{59}Fe-efflux activity was quantified in cells expressing Fpn-CFP treated with sCp or APPαBαC. These data are presented in Fig. 10. sCp has been shown to increase Fpn-dependent iron efflux and is included here as a positive control. The expectation was that changes in ^{59}Fe-efflux would parallel changes in Fpn-CFP surface expression as quantified in Fig. 9. As noted previously with respect to co-expression of Heph-YFP (see Fig. 7), increased occupancy of Fpn-CFP in the plasma membrane was not sufficient to increase in loss of ^{59}Fe in 24 h. There was, however, a modest although statistically significant increase in iron loss in cells treated with APPαBαC that was comparable with the effect seen with sCp. APPαBαC supported a comparable increase in efflux in cells expressing both Fpn-CFP and Heph-YFP. These results parallel those demonstrated in human brain microvascular endothelial cells, a model system in which nanomolar sCp or FTP supported a 2.5-fold increase in ^{59}Fe-efflux (25).

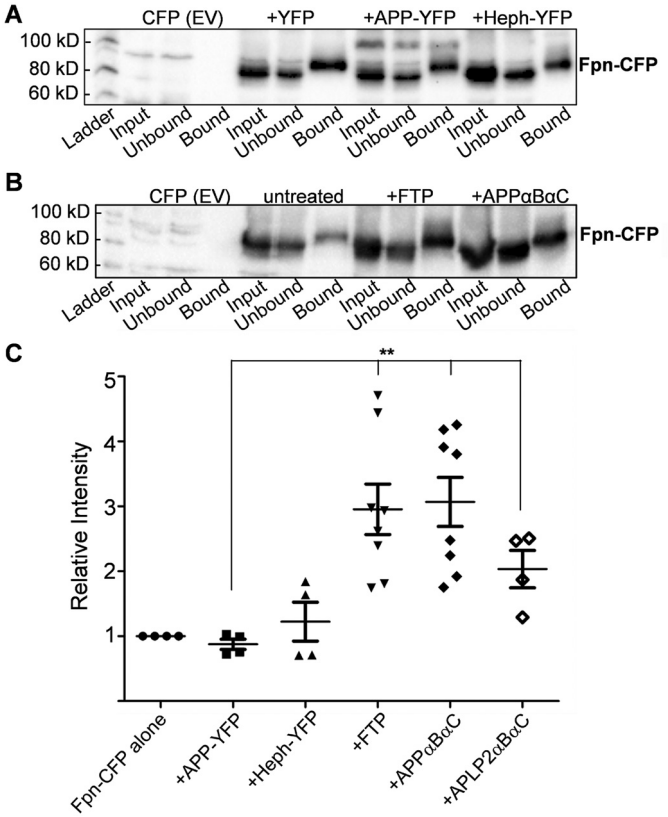

Figure 9. Surface localization of Fpn-CFP in response to endogenous expression and exogenous addition of Fpn-interacting APP orthologues. HEK293T cells were transfected to express Fpn-CFP. Indicated samples were co-transfected to express YFP (equivalent to empty vector control), APP-YFP, or Heph-YFP (*panel A*). During transfection, cells expressing Fpn-YFP alone were treated with FTP (10 nM), APPαBαC or APLP2αBαC (10 nM) (*panel B*). Proteins at the cell surface were biotinylated 48 h post-transfection using EZ-Link Sulfo-NHS-SS-Biotin, captured on Neutravidin, and eluted samples probed for Fpn-CFP. The samples probed were input; flow-through, unbound protein; bound, surface protein. *C*, bands from total and surface protein samples were quantified using Image Lab, and the intensity of the Fpn-CFP band reported relative control samples (Fpn-CFP alone). Mean ± S.D. are based on three independent experiments. **, $p < 0.01$.

Discussion

The objective of this research was 2-fold: 1) to provide direct, *in cellulo* evidence for a Fpn–Heph complex and 2) to examine

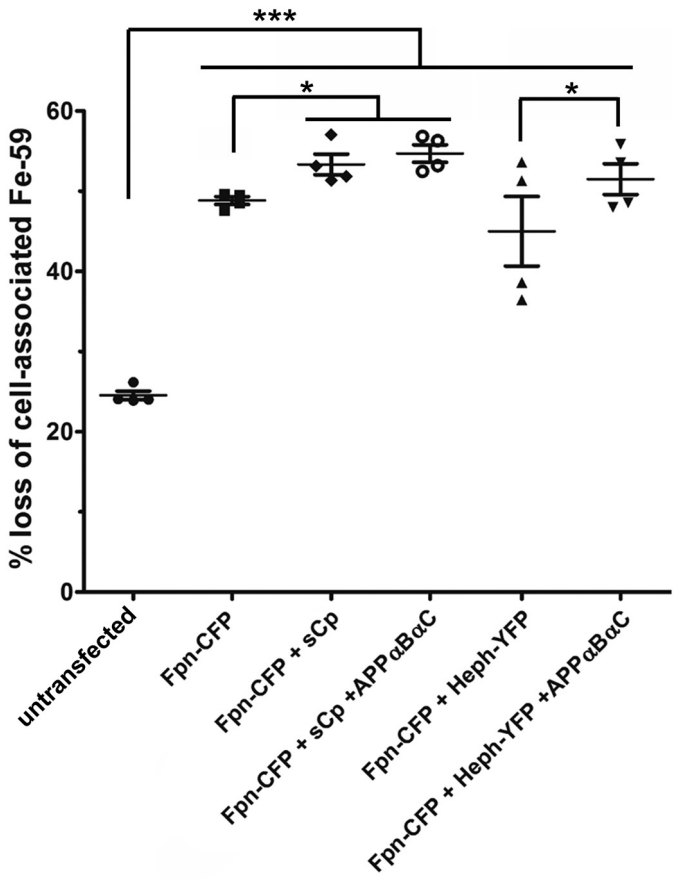

Figure 10. ^{59}Fe efflux in response to exogenous addition of Fpn-interacting proteins. HEK293T cells were transfected to express Fpn-CFP or Fpn-CFP and Heph-YFP. Cells were subsequently treated for 24 h with sCp (6.6 nM) or APPαBαC (10 nM) as indicated and then loaded for 24 h with 1 μM $^{59}FeCl_3$ (plus citrate and ascorbate). Cells were washed and $t = 0$ samples were reserved for subsequent quantification of 24 h ^{59}Fe accumulation. The remaining samples were incubated for 24 h in the continued presence of additions as indicated but minus ^{59}Fe (efflux condition). Loss of cell-associated ^{59}Fe was quantified and normalized to protein concentration; the data are presented as the percent ^{59}Fe lost compared with the $t = 0$ controls. Mean ± S.D. are based upon four biological replicates. The $p < 0.001$ values (***) are differences relative to the untransfected, untreated control. The $p < 0.05$ values (*) are differences relative to the transfected but untreated cell samples.

the cellular factors that supported the membrane occupancy and iron-efflux function of this unique mammalian iron export system, in particular the comparative effects of APP family members, APP and APLP1 and -2.

Using Fpn-CFP and Heph-YFP fusions we have demonstrated that they form a FRET pair; the confocal images indicate that this complex is found within cytoplasm-localized compartments as well as in the plasma membrane indicating that Fpn, Heph association occurs as part of the trafficking of the two proteins to the cell surface. This pattern and the FRET efficiency quantified herein is comparable with that previously reported for the Fet3, Ftr1 iron uptake complex found in *Saccharomyces cerevisiae* and in essentially all fungi and algae (57–60). Fet3, like Heph, is a Type Ia membrane protein with a multicopper ferroxidase domain that is in the extracellular space. Whereas fungal iron uptake is ferroxidase-dependent, in mammals it is iron efflux that relies on the concurrent oxidation of Fe^{2+} to Fe^{3+}.

The FRET efficiency and thus FRET-pair proximity quantified by the photobleaching protocol used did not account for the fraction of Fpn-CFP *not* in association with the acceptor-tagged Heph and thus may be an underestimate. However, one can compare our results to those obtained in experiments assessing the spatial relationship of APP in a homodimeric state (49, 61), an oligomerization that has been identified by other techniques (62, 63). The quantified FRET efficiency was 15%. This is similar to the maximum FRET observed in the Fet3-CFP, Ftr1-YFP complex in the yeast plasma membrane (59); in this complex the Fet3 ferroxidase traffics Fe^{3+} to the ferric iron permease, Ftr1, in support of the high-affinity iron uptake found in all fungi and algae (64). Both proteins have extended intracellular domains that spatially separate the donor-acceptor fluors; as these domains are truncated the FRET efficiency increases from 4 to 13% (59). Thus, the FRET value we report here for the Fpn-CFP, Heph-YFP pair of 8% is comparable with values reported for closely related systems.

Using the combination of fluorescent microscopy, surface protein biotinylation, and functional assay, we have demonstrated the opposite effects of iron supplementation *versus* copper depletion on Fpn trafficking and cell iron efflux; with respect to our reading of the literature, these results are unique in that we have combined microscopy, biochemistry, and functional assay. Our data suggest the premise that the hepcidin-independent membrane occupancy of the Fpn–Heph complex is modulated by forward trafficking rather than retarded retrograde retrieval. However, the details of the cycling of these two proteins warrant additional investigation particularly with respect to possible dependence on cell-type, for example, a barrier epithelial cell compared with a macrophage.

As noted, the experimental design in which we measured ^{59}Fe loss over 24 h did not explicitly quantify changes in the efflux *rate*; the loss of an apparent maximum of ~60% of accumulated ^{59}Fe could have represented the fraction of cell iron that was available for Fpn-mediated efflux. Another possibility is that efflux was limited by some intracellular factor other than the abundance and activity of the Fpn-Heph complex. For example, efflux could be rate-limited by the abundance of PCBP2, one of the two cytoplasmic iron chaperones found in mammalian cells (65). Data have been described indicating that PCBP2 binds to Fpn and supports Fpn-dependent iron efflux (66). This premise also warrants experimental confirmation.

We have shown data in support of the developing premise that sAPP via an REWEE motif in the amyloid precursor protein E2 domain stabilizes the iron-efflux protein, Fpn, in the plasma membrane and thereby stimulates iron efflux. This activity together with the fact that the APP transcript contains an iron-response element in its 5′ UTR suggests that among other possible physiologic functions, APP plays a role in cellular iron homeostasis. This premise is consistent also with the fact that motifs in the C terminus of sAPPα (and *not* sAPPβ) bind Fe^{2+} (67). In as much as sAPP does stabilize membrane Fpn, we conclude that sAPP plays an agonist role in iron trafficking in contrast to the antagonist role played by hepcidin. We propose that this interplay between these two proteins is a key element in brain iron homeostasis.

The key findings in support of this model are as follows. First, as discussed, we have provided fluorescence and FRET data that confirm the close relationship between Fpn and its partner ferroxidase, Heph, which has been demonstrated previously by co-immunoprecipitation. In contrast, we find no evidence of a comparable association between Fpn and full-length APP in the cell, nor does expression of APP have any influence on the surface expression of Fpn. Our conclusion that sAPP and not APP functions in iron trafficking contrasts with one report suggesting that *cell* APP (the unprocessed, native protein) stimulated Fpn-dependent iron efflux in hippocampal neurons (24), a result, however, that recently has been challenged (19). On the other hand, the results reported here in HEK293T cells are similar to those reported in brain microvascular endothelial cells (6, 25) and hippocampal neurons (19), *i.e.* stimulation of iron efflux upon addition of sAPP or the ferroportin targeting peptide from its E2 domain. That this function is associated with a processed form of APP parallels the findings that other physiologic and neuroprotective functions associated with amyloid protein family members are due to their soluble forms (29, 30).

sAPP or the recombinant αBαC helices from APP's E2 domain enhance plasma membrane expression of Fpn. This effect is quantitatively similar to that due to the addition of the specific FTP peptide previously identified in this domain that includes what appears to be the characteristic FTP element, (K/R)EWEE (24, 25, 35). This conclusion is supported by the fact that whereas the αBαC helices from APLP2 elicit the same Fpn localization as does sAPP and its E2 helical domain, αBαC helices from APLP1 do not. The likely sequence element underlying this functional difference is the REWAM motif in APLP1; previous studies have shown that a REW(E→N)E substitution suppressed the ferroportin targeting activity in sAPP (24). Thus, at least with respect to a proposed role in brain iron homeostasis, sAPP and sAPLP2 appear to be redundant. The differing effects of the (K/R)EWEE-containing species compared with the APLP1 recombinant fragment indicate also that the effects documented are specific to this sequence and not due to some nonspecific protein–protein interaction. Note that the 22-amino acid FTP sequence motif that includes the (K/R)EWEE element is 100% conserved in the β-amyloid A4 protein and isoforms across essentially all archived mammalian genomes.

Although APP is ubiquitously expressed in a wide variety of human tissues, we propose that the function of sAPP in modulating the surface expression of Fpn is restricted to the abluminal space in the brain. Here, given the reduced fluid volume, and circulation limited primarily to diffusion (68), the effective, *steady-state* concentration of sAPP *and* sCp released from cells in the neurovascular unit would be elevated compared with the concentration of either protein found in the general circulation. This would be particularly true at the points of close association between glia and the capillary endothelial cells, and between glia and neurons. We have shown also that endogenous, unprocessed APP plays no role in Fpn-dependent iron efflux from primary rat hippocampal neurons (19), a result that parallels the findings reported in the heterologous system used here.

In this context, we propose that sAPP and sCp from glia are key modulators of iron efflux into the brain across the blood-brain barrier, and from neurons (19, 28, 35); indeed, previous data from this laboratory has demonstrated that endothelial cell interleukin-6 stimulates glial cell expression and secretion of sCp into the basal space underlying the capillary endothelium (69). This model is consistent with the general view that glia play a key role in regulating overall brain metabolism. Thus, our model also suggests that the regulation of APP expression *and processing* in glia supports this iron trafficking function; this regulation, then, is an important focus of our ongoing research.

Experimental procedures

Cell culture and reagents

HEK293T cells (Cell Applications, San Diego, CA) were cultured in Dulbecco's modified Eagle's medium (Vendor info) with 10% fetal bovine serum (Gemini Bio-products, West Sacramento, CA) and $NaHCO_3$, pH 7.4. Cells were incubated in a humidified incubator at 37 °C, 5% CO_2. The culture medium was replaced every other day and cells were passaged weekly. Experiments were performed in 33-mm, 60-mm, 100-mm, or 24-well tissue culture dishes unless otherwise specified. Experiments were performed between passage 5 and 10 when cells reached ~90–95% confluence.

FTP peptides (sequence; HRERMSQVMREWEEAERQAKNL) without and with a C-terminal FLAG affinity tag (DYKDDDK) were synthesized by GenScript (Piscataway, NJ). Human soluble ceruloplasmin was purchased from GenWay Biotech, Inc. (San Diego, CA).

Generation of plasmids

A cDNA for the coding region of mouse ferroportin (Fpn) was amplified from pFpn-EGFP-N1 that was kindly provided by J. Kaplan (70). The PCR product was cloned into the XhoI and NheI sites of the pCEP4CyPet-MAMM vector (Addgene, Cambridge, MA) to obtain the Fpn-CFP construct. A cDNA for Heph (obtained also from J. Kaplan, University of Utah) was cloned into the XhoI and NotI sites of the pCEP4YPet-MAMM vector (Addgene) to obtain the Heph-YFP construct. The cDNA for mouse APP, APLP1, or APLP2 (transOMIC Technologies, Huntsville, AL) was cloned into HindIII (APP and APLP1) or XhoI (APLP2) and NheI sites of the pCEP4YPet-MAMM vector (Addgene) to obtain the APP/APLP1/APLP2-YFP constructs. Expression of all of the resulting ORFs was under the control of a cytomegalovirus promoter; none of the resulting mRNA species contained an iron response element. The constructs were transformed into DH5α *Escherichia coli* and ampicillin-resistant colonies selected. Plasmids were then purified (E.Z.N.A.® Plasmid Mini Kit I, Omega) and sequenced.

The ORF corresponding to the mouse APP αBαC helices (residues 318–408) (63) was amplified from cDNA (described above) using the primers 5′-*CGACGCCGTCCATATGTACCTGGAGACACC*-3′ (forward) and 5′-*CGTACTTCTTCAGCATGTTGGATCCTTAATGAGGCCTTGGGGGCACC*-3′ (reverse) and cloned into the NdeI and BamHI sites of the pET16b vector to generate pET16b-APPαBαC. The ORF corresponding to the mouse APLP1 αBαC helices was amplified from cDNA (described above) using the primers 5′-*CCTACTGATGGTGTGCATATGTACTTTGGCATGC*-3′ (for-

ward) and 5′-*CAGGGCCATCAGGGATCCCTAAGCCTGAGGCGGATC*-3′ (reverse) and cloned into the NdeI and BamHI sites of the pET16b vector to generate pET16b-APLP1αBαC. The ORF corresponding to the mouse APLP2 αBαC helices was amplified from cDNA (described above) using the primers 5′-*CCAACCAATGATGTTCATATGTATTTTGAGACCTCAGC*-3′ (forward) and 5′-*GTTCTCAGCACGGACGGATCCTCAAAGAGCTTGAAGAATCCG*-3′ (reverse) and cloned into the NdeI and BamHI sites of the pET16b vector to generate pET16b-APLP2αBαC. These constructs were transformed into DH5α *E. coli* and ampicillin-resistant colonies were selected. Plasmids were then purified and sequenced to verify.

Overexpression and isolation of APP, APLP1, and APLP2 αBαC helices

Overexpression of His_6-tagged APP αBαC helices was performed in the *E. coli* BL21(DE3)-RIL strain in LB at 30 °C shaking until A_{600} = 0.6–0.8, followed by induction with 0.5 mM isopropyl β-D-thiogalactosidase. The cells were collected 18 h after induction and resuspended in 20 mM sodium phosphate, pH 7.4, 0.5 M NaCl, 1 mM phenylmethylsulfonyl fluoride containing a bacterial protease inhibitor mixture. Cells were sonicated and centrifuged, and the supernatant was filtered to remove cell debris. The cell-free extract was loaded onto a HiTrap IMAC column charged with nickel (GE Healthcare) equilibrated with 20 mM sodium phosphate, pH 7.4, 0.5 M NaCl. The protein was eluted with a 0–500 mM imidazole gradient. Fractions containing His_6-tagged APPαBαC as judged by Coomassie-stained SDS-PAGE were collected, exchanged into 20 mM sodium phosphate, pH 7.4, 200 mM NaCl buffer, and concentrated. Overexpression and isolation of APLP1 and APLP2 αBαC helices followed the same protocol as described above.

HEK293T transfection

HEK293T cells were transiently transfected with one or two of the following CFP/YFP expression plasmid pairs: Fpn-CFP, Heph-YFP, APP-YFP, APLP1-YFP, APLP2-YFP. Polyethylenimine (PEI) MAX (Polysciences, Inc.) was used as the transfection reagent following an established protocol (71). Briefly DNA and PEI were diluted separately in Opti-MEM (ThermoFisher) before mixing and incubating 30 min at room temperature. The DNA/PEI mixture was added dropwise to cells and gently swirled to distribute. Experiments were performed on cells after incubation with the transfection mixture for 48 h.

Surface protein biotinylation and immunoblotting

Membrane proteins from HEK293T were biotinylated and separated from the cellular protein pool as follows. Cells grown in 60-mm tissue culture dishes were washed 2 times with PBS, treated with EZ-Link™ Sulfo-NHS-SS-Biotin to biotinylate surface proteins (ThermoFisher) for 30 min at 4 °C, washed 2 times with PBS + 0.1% BSA and 2 times with PBS. Cells were lysed by scraping in ice-cold RIPA buffer (25 mM Tris, 150 mM NaCl, 1% Nonidet P-40, 1% sodium deoxycholate, 0.1% SDS, pH 7.4) supplemented with 1× Halt protease inhibitor mixture (ThermoFisher) and incubation on ice for 15 min. The cell suspension was then centrifuged at 14,000 × *g* for 10 min at 4 °C, and the supernatant containing the biotinylated surface proteins was collected. Protein content in the supernatant was quantified, and equal amounts of protein were loaded to streptavidin spin columns (ThermoFisher). Columns were washed with ice-cold RIPA buffer, and bound biotinylated proteins were eluted using 2× SDS loading buffer (350 mM Tris-Cl, pH 6.8, 10% glycerol, 3.5% SDS, 0.004% bromphenol blue, 50 mM DTT). Biotinylated protein content was quantified, and equal amounts of protein were loaded for Western blotting.

Samples were resolved on duplicate 12% SDS-PAGE gels, and protein was transferred to PVDF membranes followed by blocking for 1 h at room temperature in either 5% BSA or 5% milk in TBST. The duplicate membranes were then incubated overnight at 4 °C with either rabbit anti-GFP (1:10,000 dilution in 3% BSA/TBST; Clontech) or rabbit anti-Fpn (1:2,000 dilution in 5% milk-TBST, gift from M. Knutson, University of Florida), and then washed and incubated with secondary anti-rabbit HRP antibody (Santa Cruz Biotechnology) (1:10,000 dilution in 3% BSA/TBST for anti-GFP or 1:4,000 dilution in 3% milk/TBST for anti-Fpn) at room temperature. Blots were developed using SuperSignal West Dura Extended Duration Substrate (ThermoScientific), then imaged using a ChemiDoc Imaging System with Image Lab software (Bio-Rad). The duplicate blots probed with the anti-Fpn antibody confirmed assignment of GFP-containing bands to Fpn-CFP; these latter blots are presented in the figures.

Fluorescence microscopy

HEK293T were fixed for 10 min with 4% paraformaldehyde and 4% sucrose in PBS. Coverslips were mounted onto glass slides using SlowFade gold antifade reagent with 4′,6-diamidino-2-phenylindole (Invitrogen). The slides were visualized using either an Axioimager epifluorescence microscope or LSM-510 Meta NLO laser scanning confocal microscope (Zeiss). The latter instrument was used exclusively for the FRET analyses. FRET efficiency was calculated using the equation,

$$E = 1 - I_{DA}/I_D \quad \text{(Eq. 1)}$$

where I_{DA} and I_D are the total donor fluorescence emission intensities in the presence and absence of energy transfer to *A*. These resulting fluorescence intensities were quantified in ROI confined to membrane-associated regions of the cell. Fluorescence images were generated using ImageJ.

^{59}Fe efflux assays

All ^{59}Fe efflux assays were performed using confluent monolayers of HEK293T grown in 24-well tissue culture dishes. Assays were performed at 37 °C in 5% CO_2 at 75 rpm. The radionuclide $^{59}FeCl_3$ was purchased from PerkinElmer Life Sciences. HEK293T were loaded for 24 h with ^{59}Fe(II) citrate (plus 500 μM BCS where applicable), washed with Dulbecco's modified Eagle's medium containing 250 μM citrate, and incubated with reagents as noted in each experiment for 0–24 h. Additions to the efflux media, where applicable (final concentrations indicated), included BCS (500 μM), FTP (10 nM), sCp (6.6 nM), APP-αBαC (10 nM), or a combination of components. Reactions were quenched with ice-cold quench buffer as described

previously (72) and lysed with radioimmune precipitation assay buffer. Lysates were assayed for ^{59}Fe and protein concentration. All counts were normalized for protein content at time 0 h prior to initiation of ^{59}Fe efflux.

Ferroxidase assay

Ferroxidase activity was quantified by the fraction of ferrous iron remaining after a 30- or 60-min incubation with a sample using ferrozine ((3-(2-pyridyl)-5,6-bis(4-phenylsulfonic acid)-1,2,4-triazine) as Fe(II) indicator (for the $(FZ)_3$-Fe(II) complex, $\epsilon(550\ nm) = 27.9\ mM^{-1}\ cm^{-1}$) (73). Soluble human ceruloplasmin was used as standard. Assays were performed in 100 mM MES buffer, pH 6.0, containing 10 mM freshly prepared FAS. Reactions were quenched by addition of ferrozine (Millipore Sigma, 100 μM final concentration) and the remaining Fe(II) quantified by absorbance at 550 nm. Sample data are presented as ferroxidase equivalents by reference to an hCp standard curve.

Statistical analysis

All statistical analyses were performed by using Prism 5.0 or 8.0 (GraphPad Software, San Diego, CA).

Author contributions—A. C. D. and D. J. K. conceptualization; A. C. D., D. K. B., B. L. S., and H. V. P. data curation; A. C. D., D. K. B., B. L. S., and H. V. P. formal analysis; A. C. D., D. K. B., B. L. S., and H. V. P. validation; A. C. D., D. K. B., and B. L. S. investigation; A. C. D., D. K. B., B. L. S., H. V. P., and D. J. K. methodology; A. C. D., D. K. B., B. L. S., and D. J. K. writing-review and editing; D. J. K. supervision; D. J. K. funding acquisition; D. J. K. writing-original draft; D. J. K. project administration.

References

1. Anderson, G. J., and Frazer, D. M. (2017) Current understanding of iron homeostasis. *Am. J. Clin. Nutr.* **106,** 1559S–1566S CrossRef Medline
2. Coffey, R., and Ganz, T. (2017) Iron homeostasis: an anthropocentric perspective. *J. Biol. Chem.* **292,** 12727–12734 CrossRef Medline
3. Rishi, G., and Subramaniam, V. N. (2017) The liver in regulation of iron homeostasis. *Am. J. Physiol. Gastrointest. Liver Physiol.* **313,** G157–G165 CrossRef Medline
4. Donovan, A., Lima, C. A., Pinkus, J. L., Pinkus, G. S., Zon, L. I., Robine, S., and Andrews, N. C. (2005) The iron exporter ferroportin/Slc40a1 is essential for iron homeostasis. *Cell Metab.* **1,** 191–200 CrossRef Medline
5. Yeh, K. Y., Yeh, M., and Glass, J. (2011) Interactions between ferroportin and hephaestin in rat enterocytes are reduced after iron ingestion. *Gastroenterology* **141,** 292–299, 299.e1 CrossRef Medline
6. McCarthy, R. C., and Kosman, D. J. (2013) Ferroportin and exocytoplasmic ferroxidase activity are required for brain microvascular endothelial cell iron efflux. *J. Biol. Chem.* **288,** 17932–17940 CrossRef Medline
7. Fuqua, B. K., Lu, Y., Darshan, D., Frazer, D. M., Wilkins, S. J., Wolkow, N., Bell, A. G., Hsu, J., Yu, C. C., Chen, H., Dunaief, J. L., Anderson, G. J., and Vulpe, C. D. (2014) The multicopper ferroxidase hephaestin enhances intestinal iron absorption in mice. *PloS One* **9,** e98792 CrossRef Medline
8. Nemeth, E., Tuttle, M. S., Powelson, J., Vaughn, M. B., Donovan, A., Ward, D. M., Ganz, T., and Kaplan, J. (2004) Hepcidin regulates cellular iron efflux by binding to ferroportin and inducing its internalization. *Science* **306,** 2090–2093 CrossRef Medline
9. Qiao, B., Sugianto, P., Fung, E., Del-Castillo-Rueda, A., Moran-Jimenez, M. J., Ganz, T., and Nemeth, E. (2012) Hepcidin-induced endocytosis of ferroportin is dependent on ferroportin ubiquitination. *Cell Metab.* **15,** 918–924 CrossRef Medline
10. Du, F., Qian, Z. M., Luo, Q., Yung, W. H., and Ke, Y. (2015) Hepcidin suppresses brain iron accumulation by downregulating iron transport proteins in iron-overloaded rats. *Mol. Neurobiol.* **52,** 101–114 Medline
11. Drakesmith, H., Nemeth, E., and Ganz, T. (2015) Ironing out ferroportin. *Cell Metab.* **22,** 777–787 CrossRef Medline
12. Rishi, G., Wallace, D. F., and Subramaniam, V. N. (2015) Hepcidin: regulation of the master iron regulator. *Biosci. Rep.* **35,** e00192 Medline
13. Wallace, D. F., McDonald, C. J., Ostini, L., Iser, D., Tuckfield, A., and Subramaniam, V. N. (2017) The dynamics of hepcidin-ferroportin internalization and consequences of a novel ferroportin disease mutation. *Am. J. Hematol.* **92,** 1052–1061 CrossRef Medline
14. Muckenthaler, M. U., Rivella, S., Hentze, M. W., and Galy, B. (2017) A red carpet for iron metabolism. *Cell* **168,** 344–361 CrossRef Medline
15. Duck, K. A., and Connor, J. R. (2016) Iron uptake and transport across physiological barriers. *Biometals* **29,** 573–591 CrossRef Medline
16. McCarthy, R. C., and Kosman, D. J. (2014) Glial cell ceruloplasmin and hepcidin differentially regulate iron efflux from brain microvascular endothelial cells. *PloS One* **9,** e89003 CrossRef Medline
17. Jiang, R., Hua, C., Wan, Y., Jiang, B., Hu, H., Zheng, J., Fuqua, B. K., Dunaief, J. L., Anderson, G. J., David, S., Vulpe, C. D., and Chen, H. (2015) Hephaestin and ceruloplasmin play distinct but interrelated roles in iron homeostasis in mouse brain. *J. Nutr.* **145,** 1003–1009 CrossRef Medline
18. Duck, K. A., Simpson, I. A., and Connor, J. R. (2017) Regulatory mechanisms for iron transport across the blood-brain barrier. *Biochem. Biophys. Res. Commun.* **494,** 70–75 CrossRef Medline
19. Ji, C., Steimle, B. L., Bailey, D. K., and Kosman, D. J. (2018) The ferroxidase hephaestinbut not amyloid precursor protein is required for ferroportin-supported iron efflux in primary hippocampal neurons. *Cell Mol. Neurobiol.* **38,** 941–954 CrossRef Medline
20. Chen, H., Huang, G., Su, T., Gao, H., Attieh, Z. K., McKie, A. T., Anderson, G. J., and Vulpe, C. D. (2006) Decreased hephaestin activity in the intestine of copper-deficient mice causes systemic iron deficiency. *J. Nutr.* **136,** 1236–1241 CrossRef Medline
21. De Domenico, I., Ward, D. M., di Patti, M. C., Jeong, S. Y., David, S., Musci, G., and Kaplan, J. (2007) Ferroxidase activity is required for the stability of cell surface ferroportin in cells expressing GPI-ceruloplasmin. *EMBO J.* **26,** 2823–2831 CrossRef Medline
22. Lee, S. M., Attieh, Z. K., Son, H. S., Chen, H., Bacouri-Haidar, M., and Vulpe, C. D. (2012) Iron repletion relocalizes hephaestin to a proximal basolateral compartment in polarized MDCK and Caco2 cells. *Biochem. Biophys. Res. Commun.* **421,** 449–455 CrossRef Medline
23. Yeh, K. Y., Yeh, M., Mims, L., and Glass, J. (2009) Iron feeding induces ferroportin 1 and hephaestin migration and interaction in rat duodenal epithelium. *Am. J. Physiol. Gastrointest. Liver Physiol.* **296,** G55–G65 CrossRef Medline
24. Duce, J. A., Tsatsanis, A., Cater, M. A., James, S. A., Robb, E., Wikhe, K., Leong, S. L., Perez, K., Johanssen, T., Greenough, M. A., Cho, H. H., Galatis, D., Moir, R. D., Masters, C. L., McLean, C., *et al.* (2010) Iron-export ferroxidase activity of β-amyloid precursor protein is inhibited by zinc in Alzheimer's disease. *Cell* **142,** 857–867 CrossRef Medline
25. McCarthy, R. C., Park, Y. H., and Kosman, D. J. (2014) sAPP modulates iron efflux from brain microvascular endothelial cells by stabilizing the ferrous iron exporter ferroportin. *EMBO Rep.* **15,** 809–815 CrossRef Medline
26. Rogers, J. T., Randall, J. D., Cahill, C. M., Eder, P. S., Huang, X., Gunshin, H., Leiter, L., McPhee, J., Sarang, S. S., Utsuki, T., Greig, N. H., Lahiri, D. K., Tanzi, R. E., Bush, A. I., Giordano, T., and Gullans, S. R. (2002) An iron-responsive element type II in the 5′-untranslated region of the Alzheimer's amyloid precursor protein transcript. *J. Biol. Chem.* **277,** 45518–45528 CrossRef Medline
27. Cho, H. H., Cahill, C. M., Vanderburg, C. R., Scherzer, C. R., Wang, B., Huang, X., and Rogers, J. T. (2010) Selective translational control of the Alzheimer amyloid precursor protein transcript by iron regulatory protein-1. *J. Biol. Chem.* **285,** 31217–31232 CrossRef Medline
28. McCarthy, R. C., and Kosman, D. J. (2015) Mechanisms and regulation of iron trafficking across the capillary endothelial cells of the blood-brain barrier. *Front. Mol. Neurosci.* **8,** 31 Medline
29. Müller, U. C., Deller, T., and Korte, M. (2017) Not just amyloid: physiological functions of the amyloid precursor protein family. *Nat. Rev. Neurosci.* **18,** 281–298 CrossRef Medline
30. Müller, U. C., and Zheng, H. (2012) Physiological functions of APP family proteins. *Cold Spring Harbor Perspect. Med.* **2,** a006288 Medline

31. Klevanski, M., Saar, M., Baumkötter, F., Weyer, S. W., Kins, S., and Müller, U. C. (2014) Differential role of APP and APLPs for neuromuscular synaptic morphology and function. *Mol. Cell Neurosci.* **61,** 201–210 CrossRef Medline
32. Weyer, S. W., Zagrebelsky, M., Herrmann, U., Hick, M., Ganss, L., Gobbert, J., Gruber, M., Altmann, C., Korte, M., Deller, T., and Müller, U. C. (2014) Comparative analysis of single and combined APP/APLP knockouts reveals reduced spine density in APP-KO mice that is prevented by APPsα expression. *Acta Neuropathol. Commun.* **2,** 36 CrossRef Medline
33. Marik, S. A., Olsen, O., Tessier-Lavigne, M., and Gilbert, C. D. (2016) Physiological role for amyloid precursor protein in adult experience-dependent plasticity. *Proc. Natl. Acad. Sci. U.S.A.* **113,** 7912–7917 CrossRef Medline
34. Hick, M., Herrmann, U., Weyer, S. W., Mallm, J. P., Tschäpe, J. A., Borgers, M., Mercken, M., Roth, F. C., Draguhn, A., Slomianka, L., Wolfer, D. P., Korte, M., and Müller, U. C. (2015) Acute function of secreted amyloid precursor protein fragment APPsα in synaptic plasticity. *Acta Neuropathol.* **129,** 21–37 CrossRef Medline
35. McCarthy, R. C., and Kosman, D. J. (2015) Iron transport across the blood-brain barrier: development, neurovascular regulation and cerebral amyloid angiopathy. *Cell. Mol. Life Sci.* **72,** 709–727 CrossRef Medline
36. Coburger, I., Dahms, S. O., Roeser, D., Gührs, K. H., Hortschansky, P., and Than, M. E. (2013) Analysis of the overall structure of the multi-domain amyloid precursor protein (APP). *PloS One* **8,** e81926 CrossRef Medline
37. Aschemeyer, S., Qiao, B., Stefanova, D., Valore, E. V., Sek, A. C., Ruwe, T. A., Vieth, K. R., Jung, G., Casu, C., Rivella, S., Jormakka, M., Mackenzie, B., Ganz, T., and Nemeth, E. (2018) Structure-function analysis of ferroportin defines the binding site and an alternative mechanism of action of hepcidin. *Blood* **131,** 899–910 CrossRef Medline
38. Anderson, G. J., Frazer, D. M., McKie, A. T., and Vulpe, C. D. (2002) The ceruloplasmin homolog hephaestin and the control of intestinal iron absorption. *Blood Cells Mol. Dis.* **29,** 367–375 CrossRef Medline
39. Chua, K., Fung, E., Micewicz, E. D., Ganz, T., Nemeth, E., and Ruchala, P. (2015) Small cyclic agonists of iron regulatory hormone hepcidin. *Bioorg. Med. Chem. Lett.* **25,** 4961–4969 CrossRef Medline
40. Fung, E., Sugianto, P., Hsu, J., Damoiseaux, R., Ganz, T., and Nemeth, E. (2013) High-throughput screening of small molecules identifies hepcidin antagonists. *Mol. Pharmacol.* **83,** 681–690 CrossRef Medline
41. Rafiee, A., Fatemi, S., Jamili, S., Ajdari, S., Riazi-Rad, F., Memarnejadian, A., and Alimohammadian, M. (2012) Cloning, expression and characterization of zebra fish ferroportin in HEK 293T cell line. *Iran J. Public Health* **41,** 79–86 Medline
42. Tselepis, C., Ford, S. J., McKie, A. T., Vogel, W., Zoller, H., Simpson, R. J., Diaz Castro, J., Iqbal, T. H., and Ward, D. G. (2010) Characterization of the transition-metal-binding properties of hepcidin. *Biochem. J.* **427,** 289–296 CrossRef Medline
43. Gonçalves, A. S., Muzeau, F., Blaybel, R., Hetet, G., Driss, F., Delaby, C., Canonne-Hergaux, F., and Beaumont, C. (2006) Wild-type and mutant ferroportins do not form oligomers in transfected cells. *Biochem. J.* **396,** 265–275 CrossRef Medline
44. Rice, A. E., Mendez, M. J., Hokanson, C. A., Rees, D. C., and Björkman, P. J. (2009) Investigation of the biophysical and cell biological properties of ferroportin, a multipass integral membrane protein iron exporter. *J. Mol. Biol.* **386,** 717–732 CrossRef Medline
45. Han, O., and Kim, E. Y. (2007) Colocalization of ferroportin-1 with hephaestin on the basolateral membrane of human intestinal absorptive cells. *J. Cell Biochem.* **101,** 1000–1010 CrossRef Medline
46. Deshpande, C. N., Ruwe, T. A., Shawki, A., Xin, V., Vieth, K. R., Valore, E. V., Qiao, B., Ganz, T., Nemeth, E., Mackenzie, B., and Jormakka, M. (2018) Calcium is an essential cofactor for metal efflux by the ferroportin transporter family. *Nat. Commun.* **9,** 3075 CrossRef Medline
47. Bajar, B. T., Wang, E. S., Zhang, S., Lin, M. Z., and Chu, J. (2016) A guide to fluorescent protein FRET pairs. *Sensors (Basel)* **16,** e1488 Medline
48. Hoppe, A., Christensen, K., and Swanson, J. A. (2002) Fluorescence resonance energy transfer-based stoichiometry in living cells. *Biophys. J.* **83,** 3652–3664 CrossRef Medline
49. Kaden, D., Voigt, P., Munter, L. M., Bobowski, K. D., Schaefer, M., and Multhaup, G. (2009) Subcellular localization and dimerization of APLP1 are strikingly different from APP and APLP2. *J. Cell Sci.* **122,** 368–377 CrossRef Medline
50. Delaby, C., Pilard, N., Gonçalves, A. S., Beaumont, C., and Canonne-Hergaux, F. (2005) Presence of the iron exporter ferroportin at the plasma membrane of macrophages is enhanced by iron loading and down-regulated by hepcidin. *Blood* **106,** 3979–3984 CrossRef Medline
51. D'Anna, M. C., Veuthey, T. V., and Roque, M. E. (2009) Immunolocalization of ferroportin in healthy and anemic mice. *J. Histochem. Cytochem.* **57,** 9–16 CrossRef Medline
52. Ross, S. L., Tran, L., Winters, A., Lee, K. J., Plewa, C., Foltz, I., King, C., Miranda, L. P., Allen, J., Beckman, H., Cooke, K. S., Moody, G., Sasu, B. J., Nemeth, E., Ganz, T., Molineux, G., and Arvedson, T. L. (2012) Molecular mechanism of hepcidin-mediated ferroportin internalization requires ferroportin lysines, not tyrosines or JAK-STAT. *Cell Metab.* **15,** 905–917 CrossRef Medline
53. Ward, D. M., and Kaplan, J. (2012) Ferroportin-mediated iron transport: expression and regulation. *Biochim. Biophys. Acta* **1823,** 1426–1433 CrossRef Medline
54. Nittis, T., and Gitlin, J. D. (2004) Role of copper in the proteosome-mediated degradation of the multicopper oxidase hephaestin. *J. Biol. Chem.* **279,** 25696–25702 CrossRef Medline
55. Chen, H., Attieh, Z. K., Dang, T., Huang, G., van der Hee, R. M., and Vulpe, C. (2009) Decreased hephaestin expression and activity leads to decreased iron efflux from differentiated Caco2 cells. *J. Cell Biochem.* **107,** 803–808 CrossRef Medline
56. Yu, Y., Wong, J., Lovejoy, D. B., Kalinowski, D. S., and Richardson, D. R. (2006) Chelators at the cancer coalface: desferrioxamine to triapine and beyond. *Clin. Cancer Res.* **12,** 6876–6883 CrossRef Medline
57. Ziegler, L., Terzulli, A., Gaur, R., McCarthy, R., and Kosman, D. J. (2011) Functional characterization of the ferroxidase, permease high-affinity iron transport complex from *Candida albicans*. *Mol. Microbiol.* **81,** 473–485 CrossRef Medline
58. Terzulli, A. J., and Kosman, D. J. (2009) The Fox1 ferroxidase of *Chlamydomonas reinhardtii*: a new multicopper oxidase structural paradigm. *J. Biol. Inorg. Chem.* **14,** 315–325 CrossRef Medline
59. Singh, A., Severance, S., Kaur, N., Wiltsie, W., and Kosman, D. J. (2006) Assembly, activation, and trafficking of the Fet3p·Ftr1p high affinity iron permease complex in *Saccharomyces cerevisiae*. *J. Biol. Chem.* **281,** 13355–13364 CrossRef Medline
60. Kosman, D. J. (2003) Molecular mechanisms of iron uptake in fungi. *Mol. Microbiol.* **47,** 1185–1197 CrossRef Medline
61. Devauges, V., Marquer, C., Lécart, S., Cossec, J. C., Potier, M. C., Fort, E., Suhling, K., and Lévêque-Fort, S. (2012) Homodimerization of amyloid precursor protein at the plasma membrane: a homoFRET study by time-resolved fluorescence anisotropy imaging. *PloS One* **7,** e44434 CrossRef Medline
62. Hoefgen, S., Coburger, I., Roeser, D., Schaub, Y., Dahms, S. O., and Than, M. E. (2014) Heparin induced dimerization of APP is primarily mediated by E1 and regulated by its acidic domain. *J. Struct. Biol.* **187,** 30–37 CrossRef Medline
63. Dahms, S. O., Könnig, I., Roeser, D., Güuhrs, K. H., Mayer, M. C., Kaden, D., Multhaup, G., and Than, M. E. (2012) Metal binding dictates conformation and function of the amyloid precursor protein (APP) E2 domain. *J. Mol. Biol.* **416,** 438–452 CrossRef Medline
64. Kosman, D. J. (2010) Redox cycling in iron uptake, efflux, and trafficking. *J. Biol. Chem.* **285,** 26729–26735 CrossRef Medline
65. Philpott, C. C., Ryu, M. S., Frey, A., and Patel, S. (2017) Cytosolic iron chaperones: proteins delivering iron cofactors in the cytosol of mammalian cells. *J. Biol. Chem.* **292,** 12764–12771 CrossRef Medline
66. Yanatori, I., Richardson, D. R., Imada, K., and Kishi, F. (2016) Iron export through the transporter ferroportin 1 is modulated by the iron chaperone PCBP2. *J. Biol. Chem.* **291,** 17303–17318 CrossRef Medline
67. Bousejra-ElGarah, F., Bijani, C., Coppel, Y., Faller, P., and Hureau, C. (2011) Iron(II) binding to amyloid-β, the Alzheimer's peptide. *Inorg. Chem.* **50,** 9024–9030 CrossRef Medline
68. Hladky, S. B., and Barrand, M. A. (2014) Mechanisms of fluid movement into, through and out of the brain: evaluation of the evidence. *Fluids Barriers CNS* **11,** 26 CrossRef Medline

69. McCarthy, R. C., and Kosman, D. J. (2014) Activation of C6 glioblastoma cell ceruloplasmin expression by neighboring human brain endothelia-derived interleukins in an *in vitro* blood-brain barrier model system. *Cell Commun. Signal.* **12,** 65 CrossRef Medline
70. De Domenico, I., Ward, D. M., Nemeth, E., Vaughn, M. B., Musci, G., Ganz, T., and Kaplan, J. (2005) The molecular basis of ferroportin-linked hemochromatosis. *Proc. Natl. Acad. Sci. U.S.A.* **102,** 8955–8960 CrossRef Medline
71. Longo, P. A., Kavran, J. M., Kim, M. S., and Leahy, D. J. (2013) Transient mammalian cell transfection with polyethylenimine (PEI). *Methods Enzymol.* **529,** 227–240 CrossRef Medline
72. McCarthy, R. C., and Kosman, D. J. (2012) Mechanistic analysis of iron accumulation by endothelial cells of the BBB. *Biometals* **25,** 665–675 CrossRef Medline
73. Stookey, L. L. (1970) Ferrozine: a new spectrophotometric reagent for iron. *Anal. Chem.* **42,** 779–781 CrossRef